14.1

A HYBRID COMPUTATIONAL APPROACH FOR TURBULENT COLLISION-COALESCENCE OF CLOUD DROPLETS

B. Rosa[1,*], Lian-Ping Wang[1,†], and Wojciech W. Grabowski[2]

[1] Department of Mechanical Engineering, University of Delaware, Newark, Delaware 19716-3140, USA

[2] Mesoscale and Microscale Meteorology Division, National Center for Atmospheric Research
PO Box 3000, Boulder, Colorado 80307-3000, USA

Abstract

While it has long been speculated that air turbulence could accelerate the collision-coalescence of cloud droplets and as such promotes the formation of warm rain, progress has been very slow in quantifying the turbulence effects. This results from the complexity of the problem and the lack of quantitative research tools. In this talk, we will report on an on-going, systematic effort to quantify various effects of turbulence on the rate of collision-coalescence of small cloud droplets, including (1) the enhanced relative motion due to differential acceleration and shear effects, (2) enhanced average pair density due to local clustering of droplets, and (3) enhanced collision efficiency due to turbulent fluctuations.

Recently, we have developed a Hybrid Direct Numerical Simulation (HDNS) approach to treat the motion and interactions of a large number of particles suspended in a turbulent flow. The HDNS approach integrates an improved superposition method for the disturbance flows due to droplets into a pseudospectral simulation of undisturbed air turbulence. This allows, for the first time, the direct incorporation of hydrodynamic interactions within DNS and computations from first principles of statistical information related to collision-coalescence. We are currently looking into various methods to further improve the HDNS approach in order to account for near-field lubrication forces and non-continuum effects. Here we present some representative results that we have obtained, to illustrate the capabilities and potential of the HDNS approach.

1. INTRODUCTION

The collision-coalescence of cloud droplets moving under gravity in a turbulent air is central to cloud microphysics and precipitation formation (Pruppacher and Klett 1997). In this application, the volume fraction ϕ of liquid droplets is quite small (e.g., on the order of 10^{-5} or less), yet the local hydrodynamic (or aerodynamic) interactions of droplets must be considered since the growth of droplets by the collision-coalescence process is of the central concern. In this type of systems, a unique *three-way coupling* must be considered: (a) the carrier-flow turbulence affects the motion of the droplets through the interfacial viscous drag; (b) the motion of each droplet can be affected by the presence of other droplets in the system, either through the strong local near-field binary hydrodynamic interaction or by the cumulative many-body, long-range interactions; and (c) the background carrier-fluid turbulence can also affect the hydrodynamic interactions as the background turbulence defines both the far-field conditions and the local environment for the hydrodynamic interactions. Recent experimental (Aliseda *et al.* 2003) and numerical (Wang *et al.* 2006) studies reveal that this three-way interactions must be carefully and systematically considered in these systems. In this paper, the terms particles and droplets are used interchangeably, so are the terms hydrodynamic interaction and aerodynamic interaction.

Without droplet collisions, these systems can be treated with the usual one-way coupling assumption (Crowe *et al.* 1998; Elghobashi 1994), provided that the size of the droplets is much smaller than the Kolmogorov scale of the carrier-fluid turbulence. On the other hand, when the level of carrier-fluid turbulence is very weak, the hydrodynamic interactions of a dilute suspension are relatively well understood in such field as suspension mechanics or microhydrodynamics (Batchelor 1972, 1982; Hinch 1988; Kim and Karrila 1991; Nicolai *et al.* 1995; Davis 1996; Ramaswamy 2001). The situation when both the hydrodynamic interactions and the background turbulence must be simultaneously considered is the subject of this paper, and currently, to the best knowledge of the authors, there is no rigorous theoretical and computational treatment of such systems. Here we report a

* On leave from Institute of Geophysics, Warsaw University, Poland.

† Corresponding author's address: Lian-Ping Wang, Department of Mechanical Engineering, 126 Spencer Laboratory, University of Delaware, Newark, Delaware 19716-3140, USA. E-mail: lwang@me.udel.edu

first step toward developing a rigorous computational approach for a three-way coupling system.

The motivation for this research is the need to understand and quantify the effect of air turbulence on the collision rates of droplets in atmospheric warm clouds (Wang *et al.* 2005b). The topic has received much attention in recent years (see reviews by Pinsky and Khain (1997), Vaillancourt and Yau (2000), Shaw (2003)). In warm clouds, the mass loading ratio is on the order of 10^{-3} or less, and the size of cloud droplets ($5 \sim 50\ \mu m$) is typically one to two orders of magnitude smaller than the Kolmogorov scale ($\sim 1\ mm$) of the air turbulence; the effect of the droplets on the airflow momentum can be safely neglected. We must note that there could still be a significant energy coupling between the dispersed phase and the carrier fluid if the net rate of condensation or evaporation of water content is large enough to cause a significant latent heat release. In this research, we treat the airflow as nearly adiabatic and inter-phase energy coupling is not considered. The hydrodynamic interactions must be considered as we are concerned with the growth of droplets caused by collision-coalescence. Therefore, while we assume one-way coupling at the scale of undisturbed carrier flow (>1 mm), we do consider all couplings at the scale of droplet diameter (<0.1 mm). An underlying assumption is that the undisturbed or background turbulence is decoupled from the disturbance flows due to the separation in length scales of the two types of flow fields. We note, however, that the disturbance flows are strongly affected by the background turbulence.

With the assumptions mentioned above, we have recently introduced a hybrid approach Wang *et al.* (2005b); Ayala *et al.* (2006); Wang *et al.* (2006) that is similar in concept to the superposition method often used to model collision efficiency in cloud microphysics (Langmuir 1948; Shafrir and Neiburger 1963; Beard and Grover 1974; Lin and Lee 1975; Pinsky et al. 1999), but is improved to explicitly consider the no-slip boundary conditions on the surface of each droplet Wang et al. (2005a). This hybrid approach solves the background turbulent flow by the pseudo-spectral method (Moin and Mahesh 1998) with a large-scale forcing, and utilizes the improved superposition method to embed analytically the local, small-scale (10 μm to 1 mm) disturbance flows induced by the particles. This hybrid representation is then used to study the combined effects of hydrodynamic interactions and airflow turbulence on the motion and collisions of cloud droplets. The hybrid approach should be viewed as a first step as far as the treatment of local hydrodynamic interactions is concerned. More rigorous treatments in the suspension mechanics such as the Stokesian dynamics (Brady and Bossis 1988) and other improved multipole methods (Sangani and Mo 1996; Ichiki and Brady 2001; Sierou and Brady 2001; Ichiki 2002) are appropriate if more accuracy is desired. Keeping the treatment of hydrodynamic interactions simple at this stage helps with the computational efficiency of the approach.

2. THE HYBRID DNS APPROACH

For the problem of droplets moving in a turbulent cloud, the droplets can be considered as a system of heavy particles carried by a turbulent airflow field $\mathbf{U}(\mathbf{x},t)$. Typical droplet volume fractions are on the order of $O(10^{-6})$ and mass-loading on the order of 10^{-3}. Therefore, while the flow can affect the motion of droplets, the background air turbulence is not affected by the presence of the droplets (one-way coupling). The droplet size is typically one to two orders of magnitude smaller than the smallest length scale of the turbulence (the Kolmogorov length scale, η). In a stagnant fluid, the disturbance flow due to a droplet could extend up to a region about 50 times the droplet radius (Lin and Lee 1975, 1976). This length is on the order of the Kolmogorov length scale of the airflow turbulence or less. The particle Reynolds number is on the order of 0.01 to 1.0. As a first step towards the modeling of hydrodynamic interactions, the disturbance flow will be assumed to be a Stokes flow.

The background air turbulence $\mathbf{U}(\mathbf{x},t)$ is simulated by solving the Navier-Stokes equation directly. A large number (N_p) of small droplets are introduced into the computational domain, with velocities $\mathbf{V}^{(k)}(t)\ \ (k = 1, .., N_p)$. In our pseudospectral DNS of the background turbulence, the grid spacing is typically twice the Kolmogorov length scale, $\Delta x \sim 2\eta$. Clearly, the disturbance flows due to droplets are not resolved by the DNS grid. The presence of the N_p droplets together will cause a disturbance flow field $\widetilde{\mathbf{u}}(\mathbf{x},t)$ which may be thought as a superposition of the N_p very localized Stokes flows surrounding the N_p droplets. Therefore, $\widetilde{\mathbf{u}}(\mathbf{x},t)$ depends on the locations of all N_p droplets and their relative motion to the turbulent fluid.

The flow field experienced by a droplet is then the combination of the undisturbed turbulent flow $\mathbf{U}(\mathbf{x},t)$ and the disturbance flow $\widetilde{\mathbf{u}}(\mathbf{x},t)$ but with its own disturbance flow removed. The combined flow field, $\widetilde{\mathbf{U}}(\mathbf{x},t) \equiv \mathbf{U}(\mathbf{x},t) + \widetilde{\mathbf{u}}(\mathbf{x},t)$, is referred to as the composite flow field. The key element here is the proper and optimum specification of $\widetilde{\mathbf{u}}(\mathbf{x},t)$, provided that $\mathbf{U}(\mathbf{x},t)$ is known.

Since the Stokes disturbance flows are each governed by the linear Stokes equation, they can be superimposed to still satisfy the same Stokes equation locally (Wang et al. 2005a). This is the physical basis of the superposition method (Langmuir 1948; Pruppacher and Klett 1997). The challenge is to satisfy the no-slip boundary conditions for all the particles in the system. Wang et al. (2005a) recognized that, by optimizing the magnitude of the disturbance flow experienced by each particle, it is possible to satisfy the no-slip boundary condition on the surface of each particle when averaged over the surface of the particle.

Specifically, the fluid velocity of the composite flow at the center of each particle is equal to the velocity of that particle. This requirement leads to a more accurate representation of the force acting on a particle due to the disturbance flows by all other particles than the original superposition method.

In a turbulent carrier flow, the disturbance flow field in a system containing N_p small particles can be written as

$$\widetilde{\mathbf{u}}(\mathbf{x},t)=\sum_{k=1}^{N_p}\mathbf{u}_S\left(\mathbf{r}^{(k)};a^{(k)},\mathbf{V}^{(k)}-\mathbf{U}(\mathbf{Y}^{(k)},t)-\mathbf{u}^{(k)}\right), \tag{1}$$

where

$$\begin{aligned}\mathbf{u}_S(\mathbf{r}^{(k)};a^{(k)},\mathbf{V_p}^{(k)}) \equiv & \left[\frac{3}{4}\frac{a^{(k)}}{r^{(k)}}-\frac{3}{4}\left(\frac{a^{(k)}}{r^{(k)}}\right)^3\right]\frac{\mathbf{r}^{(k)}}{(r^{(k)})^2}(\mathbf{V_p}^{(k)}\cdot\mathbf{r}^{(k)}) \\ & +\left[\frac{3}{4}\frac{a^{(k)}}{r^{(k)}}+\frac{1}{4}\left(\frac{a^{(k)}}{r^{(k)}}\right)^3\right]\mathbf{V_p}^{(k)}\end{aligned} \tag{2}$$

represents the Stokes disturbance flow due to the $k-$th droplet of radius $a^{(k)}$ moving at velocity $\mathbf{V_p}^{(k)}$ in an otherwise quiescent fluid, and $\mathbf{r}^{(k)}\equiv\mathbf{x}-\mathbf{Y}^{(k)}$. Here $\mathbf{Y}^{(k)}$ is the instantaneous location of the $k-$th droplet.

Eq. (1) contains explicitly the disturbance flow velocity $\mathbf{u}^{(k)}$ at the location $\mathbf{Y}^{(k)}$ of the $k-$th droplet, due to all other droplets in the system. In Eq. (1), the combination $[\mathbf{V}^{(k)}-\mathbf{U}(\mathbf{Y}^{(k)},t)-\mathbf{u}^{(k)}]$ represents the relative velocity between the $k-$th droplet and the composite flow $\widetilde{\mathbf{U}}(\mathbf{x},t)$, excluding the disturbance flow due to the $k-$th droplet itself. Namely, $\mathbf{u}^{(k)}$ represents the disturbance flow velocity due to all droplets except the $k-$th droplet, at the location of the $k-$th droplet. $\mathbf{u}^{(k)}$ is determined by applying the center-point approximation (Wang et al. 2005a) to the boundary conditions $\widetilde{\mathbf{U}}(|\mathbf{r}^{(k)}|=a^{(k)},t)=\mathbf{V}^{(k)}$, yielding

$$\mathbf{u}^{(k)}=\underbrace{\sum_{m=1}^{N_p}}_{m\neq k}\mathbf{u}_S\left(\mathbf{d}^{(mk)};a^{(m)},\mathbf{V}^{(m)}-\mathbf{U}(\mathbf{Y}^{(m)},t)-\mathbf{u}^{(m)}\right), \tag{3}$$

for $k=1,2,...,N_p$, where $\mathbf{d}^{(mk)}\equiv\mathbf{Y}^{(k)}-\mathbf{Y}^{(m)}$. Therefore, $\mathbf{u}^{(k)}$ is a function of the background flow field and, the instantaneous locations and velocities of *all* particles. Eq. (3) implies that each disturbance flow velocity component at the location of the *k*-th particle will depend on all the disturbance flow velocity components of all other particles. Eq. (3) is a large linear system of dimension $3N_p$.

Since the Stokes flow induced by the *m*-th particle decays with $\mathbf{d}^{(mk)}$ as $a^{(m)}/d^{(mk)}$, as an approximation and also for computational efficiency, we truncate the right hand side of Eq. (3) at $d_{(mk)}/a_m=H$, or only contributions to the summation from neighboring particles with $d_{(mk)}/a_m\leq H$ are considered. Physically, the dimensionless truncation radius H should be made on the order of $(Re_p)^{-1}$ as the far-field disturbance flow can be better modelled by the Oseen's equation (Kim and Karrila 1991; Noh and Fernando 1993), where Re_p is the particle Reynolds number. The screening mechanism related to the fluid inertia (Koch and Shaqfeh 1991; Ladd 1996; Brenner 1999) implies that, if the inter-particle separation is larger than the flow Kolmogorov scale, the flow Kolmogorov scale could also affect the truncation radius H. We speculate that, for a dilute turbulent suspension considered in our paper, the truncation radius will depend on both the particle size and the flow Kolmogorov scale, the exact nature of these dependences is a topic for future research. As a first step, in this study the truncation radius H is determined by a combined consideration of numerical accuracy and computational efficiency. The efficient cell-index method, with cell size equal to the truncation radius $H\times\max(a_1,a_2)$, and the concept of linked lists (Allen and Tildesley 1987) are used here to quickly identify all the pairs participating in hydrodynamic interactions.

The drag force acting on the *k*-th particle due to the interactions with the turbulent flow field and the disturbance flow field can be rigorously shown to be (Wang et al. 2005a)

$$\mathbf{D}^{(k)}(t)=-6\pi\mu a_k\left[\mathbf{V}^{(k)}(t)-\left(\mathbf{U}(\mathbf{Y}^{(k)}(t),t)+\mathbf{u}^{(k)}\right)\right]. \tag{4}$$

Therefore, the equation of motion of any given particle "k" is

$$\frac{d\mathbf{V}^{(k)}(t)}{dt}=-\frac{\mathbf{V}^{(k)}(t)-\left(\mathbf{U}(\mathbf{Y}^{(k)}(t),t)+\mathbf{u}^{(k)}\right)}{\tau_p^{(k)}}-\mathbf{g}, \tag{5}$$

$$\frac{d\mathbf{Y}^{(k)}(t)}{dt}=\mathbf{V}^{(k)}(t), \tag{6}$$

where $\tau_p^{(k)}=2\rho_p(a^{(k)})^2/(9\mu)$ is the particle inertial response time, ρ_p is the density of the particle, and μ is the air dynamic viscosity. Without the disturbance flow, there are two important governing parameters for the motion of any particle (Wang and Maxey 1993): the first is the Stokes number defined as $St\equiv\tau_p/\tau_k$, the ratio of particle response time to flow Kolmogorov time τ_k; the second is the nondimensional terminal velocity defined as $S_v\equiv(\tau_p|\mathbf{g}|)/v_k$, the ratio of particle terminal velocity to the flow Kolmogorov velocity v_k.

In both Eqs. (4) and (5), the disturbance flow velocity experienced by each particle, $\mathbf{u}^{(k)}$, plays the central role.

What we have formulated is a hybrid DNS approach in which the disturbance flow is represented analytically while the undisturbed turbulent flow is solved numerically using an accurate pseudospectral method. In this approach, the disturbance flows will incorporate naturally the droplet-droplet hydrodynamic interactions when droplets are in close proximity on the scale of droplet diameter.

At each time step the following procedure is implemented:

1. Advance the undisturbed fluid turbulence field $\mathbf{U}(\mathbf{x}, t)$ using a pseudo-spectral method;
2. Interpolate the undisturbed fluid velocities at the locations of the droplets, $\mathbf{U}(\mathbf{Y}^{(k)}, t)$;
3. Solve the disturbance flow velocity $\mathbf{u}^{(k)}$ experienced by each droplet;
4. Advance the velocities and locations of the droplets;
5. Detect droplet-droplet collision events and calculate relevant kinematic and dynamic properties (Wang *et al.* 2005b) as necessary.

Typically, we consider a bidisperse suspension of $N_p/2$ droplets of radius a_1 and $N_p/2$ droplets of radius a_2. The simulation considers all hydrodynamic interactions (i.e., $1-1$, $1-2$, $2-2$), where $1-1$ denotes hydrodynamic interactions among size-1 particles, $1-2$ denotes hydrodynamic interactions of size-1 particles with size-2 particles, and $2-2$ hydrodynamic interactions among size-2 particles. Further implementation details of the HDNS approach are discussed thoroughly in Ayala et al. (2006).

3. RESULTS FROM HDNS SIMULATIONS

In this section, we discuss representative results that we have obtained with the HDNS approach, to illustrate a few coupled effects of hydrodynamic interactions and air turbulence on the relative motion of droplet pairs as well as on the motion of a single droplet in a turbulent suspension. The purpose here is to demonstrate the capabilities and potential of the approach, as well as the need to further develop the approach in the future. More complete discussions of the results are found in Wang *et al.* (2005b), Ayala (2005), Ayala *et al.* (2006), and Wang *et al.* (2006).

3..1 Enhanced sedimentation

We shall first discuss the motion of a single droplet in a suspension. Even without the background air turbulence, a droplet may be affected by the disturbance flows of other droplets, and as a result, can settle on average at a velocity larger than its terminal velocity. The slow decay of the Stokes disturbance flow implies that the long-range manybody hydrodynamic interactions can cause an increase in the average vertical velocity whose magnitude is proportional to the volume fraction of the droplets and the square of the truncation radius H in the HDNS representation (Batchelor 1972; Hinch 1988). This is discussed in detail in Wang *et al.* (2006) who also developed a theory to predict the mean velocity observed in HDNS simulations. Table 1 provides some typical results in a bidisperse suspension without the background air turbulence. The rows from top to bottom in Table 1 are the droplet radii in the bidisperse system, the volume fraction for each size, the terminal velocity for each size, observed increase in sedimentation in HDNS, and the theoretical predictions given by Wang *et al.* (2006).

When the background air turbulence is switched on, we find two additional enhancements in the average velocity. The first is the preferential sweeping associated with the local preferential concentrations as shown in Wang and Maxey (1993). We also find a second enhancement due to the coupling of hydrodynamic interactions and preferential concentration, since the effect of hydrodynamic interactions is governed by the local pair concentration. This is demonstrated in Fig. 1 where we show the average vertical velocity for each size in a bidisperse suspension, for three different cases. In the first case (NT-AI), the background air turbulence is switched off but the local hydrodynamic interactions are turned on. In the second case (T-NAI), the background air turbulence is switched on but the hydrodynamic interactions are ignored. In the third case (T-AI), both the background air turbulence and the local hydrodynamic interactions are activated. The results show that the enhanced settling for the third case is larger than the sum of the enhanced settling for the first two cases (Table 2). A detailed discussion of these results and their interpretation are given in Wang et al. (2006).

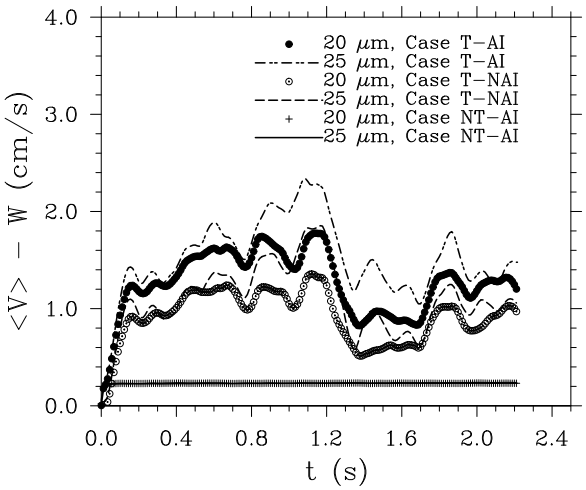

Figure 1: The difference between the quasi-steady average settling velocity and the terminal velocity, $\langle V_3^{(\alpha)} \rangle - W^{(\alpha)}$, as a function of time for $\epsilon = 400\ cm^2/s^3$.

The enhanced settling due to coupled hydrodynamic interactions and turbulence has been observed in the experimental study of Aliseda et al (2002), and is

$(a^{[1]}, a^{[2]})(\mu m)$	(20,25)	(20,30)	(20,50)	(30,50)
$\phi^{[1]}$	$4.33e-6$	$3.46e-6$	$4.33e-6$	$1.46e-5$
$\phi^{[2]}$	$8.45e-6$	$1.17e-5$	$6.76e-5$	$6.76e-5$
$V_3^{[1]}$ (cm/2)	5.478 ± 0.018	5.721 ± 0.003	13.421 ± 0.004	20.300 ± 0.005
$V_3^{[2]}$ (cm/2)	8.370 ± 0.023	12.173 ± 0.002	41.212 ± 0.046	41.973 ± 0.041
$V_3^{[1]} - W^{[1]}$ (cm/2)	0.348 ± 0.018	0.591 ± 0.003	8.290 ± 0.004	8.754 ± 0.005
$V_3^{[2]} - W^{[2]}$ (cm/2)	0.354 ± 0.023	0.631 ± 0.002	9.149 ± 0.046	9.910 ± 0.041
$V_3^{[1]} - W^{[1]}$ (cm/2), Theory	0.336	0.570	8.189	8.870
$V_3^{[2]} - W^{[2]}$ (cm/2), Theory	0.336	0.571	8.198	8.742

Table 1: Comparison of the simulated settling velocity with theory in still air, for $H = 50$.

	Case NT-AI	Case T-NAI	Case T-AI
$\langle V_3^{[1]} \rangle - W^{[1]}$: HDNS	0.2309	1.0941	1.5226
$\langle V_3^{[1]} \rangle - W^{[1]}$: Theory	0.2240	–	–
$\langle V_3^{[2]} \rangle - W^{[2]}$: HDNS	0.2315	0.9114	1.2641
$\langle V_3^{[2]} \rangle - W^{[2]}$: Theory	0.2238	–	–
$\sqrt{\langle (V_3^{[1]} - \langle V_3^{[1]} \rangle)^2 \rangle}$: HDNS	0.2648	9.62171	9.63413
$\sqrt{\langle (V_3^{[1]} - \langle V_3^{[1]} \rangle)^2 \rangle}$: Theory	0.2574	–	–
$\sqrt{\langle (V_3^{[2]} - \langle V_3^{[2]} \rangle)^2 \rangle}$: HDNS	0.2560	9.73207	9.73594
$\sqrt{\langle (V_3^{[2]} - \langle V_3^{[2]} \rangle)^2 \rangle}$: Theory	0.2580	–	–

Table 2: Results for the increased settling velocities (cm/s). All HDNS data were averaged over time from $t = 0.25$ s to $t = 2.20$ s. $\epsilon = 400\ cm^2/s^3$.

only qualitatively understood at present. When scaled with the realistic liquid water content (i.e., 1 g/m^3) in atmospheric clouds, the relative increase in the settling rate is about 2% to 3% and should be viewed as a small change. Since there is a distinct difference in Reynolds number between the HDNS airflow and the atmospheric turbulence, the question of whether this change increases with flow Reynolds number should be studied in the future. This Reynolds number dependence is related to the issue of the Reynolds number dependence of the radial distribution function (*e.g.*, Collins and Keswani 2004). The results of Yang and Shy (2005) on increased settling rate of solid particles in turbulent air appear to suggest a strong flow Reynolds number dependence. In engineering applications where the volume fractions of droplets and flow dissipation rates are much higher, the level of increase in the settling rate could be much more significant (Aliseda *et al.* 2003; Yang and Shy 2005). For example, in the experiments of Aliseda *et al.* (2003) the flow dissipation rates are one to two orders of magnitude higher. Under a similar level of volume fractions, Aliseda *et al.* (2003) found a much higher level of increased settling. The underlying mechanisms are essentially the same as these discussed above. A direct comparison with the data of Aliseda *et al.* (2003) would require a further parametric study of the turbulent sedimentation for different droplet size combinations and flow dissipation rates as well as the use of a polydisperse size distribution.

3..2 Relative motion and collision efficiency

Now we discuss some results related to a pair of droplets. Many authors have studied the hydrodynamic interaction effects on the collisions of two isolated particles settling in a stagnant fluid (Shafrir and Neiburger 1963; Lin and Lee 1975; Davis and Sartor 1967; Klett and Davis 1973). This can be viewed as a special case in our approach and thus can be used as a consistency validation test for the implementation of our approach.

The parameter used to measure the hydrodynamic interaction effects on the collision of two particles is the collision efficiency E_{12}. For the case of two isolated particles settling in a stagnant fluid, E_{12}

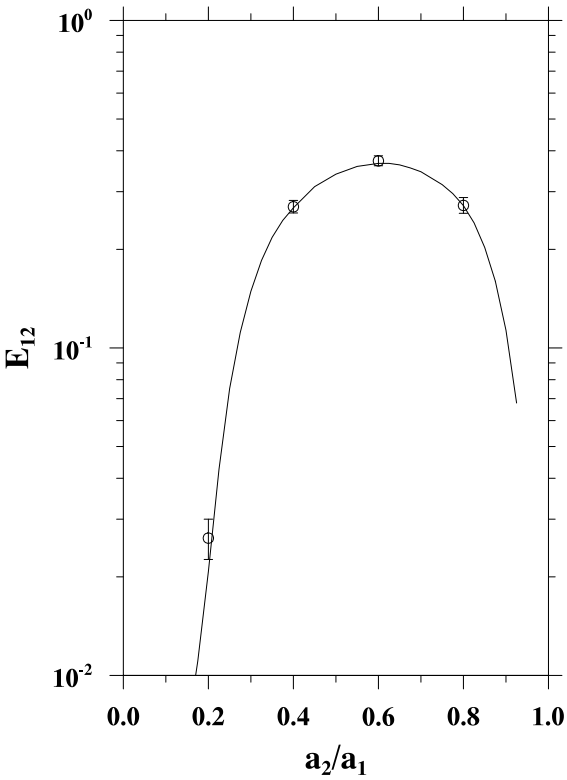

Figure 2: A benchmark problem typically used in cloud physics community to measure hydrodynamic interaction effects. The larger particle in the test is a water droplet of a_1=25 μm. The fluid is stagnant. The solid line represents collision effi ciency E_{12} obtained using Eq. (7). The dots are numerical results based on Eq. (8) using our general approach.

can be computed as (Pruppacher and Klett 1997)

$$E_{12} = \frac{y_c^2}{R^2} \tag{7}$$

where the geometric collision radius R is the sum of the radii of two colliding particles, $R = a_1 + a_2$; y_c is the far-field, off-center horizontal separation of the grazing trajectory of the smaller particle relative to the larger particle. As a result of hydrodynamic interactions, y_c is smaller than R. In our general approach, a large number of particles are simultaneously considered with many-body interactions, E_{12} is then the ratio of number of collisions with hydrodynamic interactions to the number of collisions when the hydrodynamic interactions are completely ignored

$$E_{12} = \frac{\text{Number of collisions with HI}}{\text{Number of collisions without HI}} \tag{8}$$

To obtain the collision efficiency based on equation (7), we developed a test code similar to previous studies of Klett & Davis (Klett and Davis 1973) and Lin & Lee (Lin and Lee 1975). The trajectories of two particles falling under gravity in a stagnant fluid are numerically integrated. The initial far-field off-center horizontal separations was varied until the grazing trajectory was found. The hydrodynamic interactions between the particle pair were modeled using the same improved superposition method (Wang et al. 2005a).

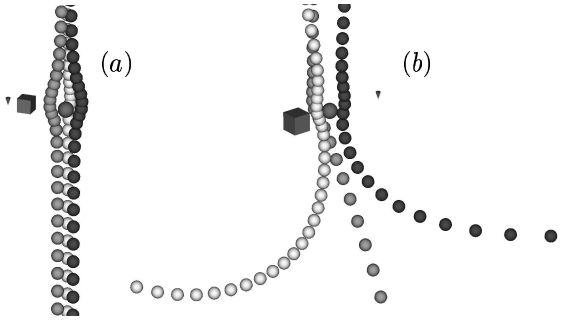

Figure 3: Three grazing trajectories of 20 μm water droplet relative to 25 μm water droplet. (a) without turbulence, (b) turbulence at ϵ=400 cm^2/s^3. The time interval for visualization was set to about 42% the inertial response time of the 20 μm droplet. The small cube in (a) has edge length equal to collision radius, while the small cube in (b) has edge length equal to 10% fbw Kolmogorov length scale. The small cone indicates the direction of gravity.

Fig. 2 shows the results from the two different approaches. The solid line represents E_{12} obtained using Eq. (7), while the dots are numerical results using our general approach. In this test, the large particle is a water droplet of a_1=25 μm in radius. In our general code, turbulence was deactivated to allow the droplets to settle under gravity and hydrodynamic interactions only. Four different cases with a_2/a_1=0.2, 0.4, 0.6, and 0.8 were considered. An excellent agreement is observed between the general approach and the simple approach. This is expected as the volume concentration of particles is very low ($\sim 10^{-6}$) so two-particle interactions dominate hydrodynamic interactions in the system.

Fig. 3 illustrates the hydrodynamic interactions between two particles using our hybrid DNS approach for identical parameter setting but with the background turbulence switched off and on. Here the three trajectories of the smaller particles relative to the large particles were selected with a minimum separation distance less than 1% of the collision radius. They can be viewed as relative grazing trajectories. An important observation is that while the relative motion is nearly vertical when there is no turbulence, the trajectories are strongly curved for the turbulent flow case and as such pairs may approach from any relative directions in the far field, making the use of Eq. (7) inapplicable as a definition of collision efficiency. In all cases the trajectories become curved when the small particle is at a close proximity of the larger particle, due to the hydrodynamic interactions. Fig. 3b shows that our approach captures both the effects of the background turbulence and hydrodynamic interactions on the relative motion of droplets.

The HDNS approach allows us to obtain kinematic statistics such as the relative velocity and radial distribution function. Recently, Wang *et al.* (2005b)

showed that the following general formulation

$$\Gamma_{12} = 2\pi R^2 \langle |w_r|(r=R)\rangle g_{12}(r=R), \qquad (9)$$

remains valid when a geometric effect due to the non-overlap of droplets is taken into account. Here w_r is the radial relative velocity and g_{12} is the radial distribution function (Sundaram and Collins 1997; Wang *et al.* 2000). Wang *et al.* (2005b) reported results on the effects of hydrodynamic interactions on the relative motion and radial distribution function. They found that hydrodynamic interactions become less effective in changing the relative radial velocity in a turbulent flow, when compared to the pure hydrodynamical-gravitational problem. This is the main reason that turbulence enhances the collision efficiency, in addition to augment the geometric collision rate. They also observed that hydrodynamic interactions increases the nonuniformity of near-field pair density distribution, resulting in higher radial distribution function at contact when compared to the geometric collision case.

To separate the effect of turbulence on collision efficiency from the previously observed effect of turbulence on geometric collision rate, we define two enhancement factors. The first measure the effect of turbulence on the geometric collision rate

$$\eta_{\rm G} = \frac{\Gamma_{12}(\text{No HI})}{\Gamma^{\rm g}_{12}(\text{No HI})}, \qquad (10)$$

where $\Gamma^{\rm g}_{12}(\text{No HI})$ is the geometrical gravitational collision kernel. Here "No HI" indicates hydrodynamic interactions are ignored. The second is the ratio of collision efficiency in a turbulent flow to that for the hydrodynamical-gravitational problem

$$\eta_{\rm E} = \frac{E_{12}}{E^{\rm g}_{12}}. \qquad (11)$$

Figure 4 shows the enhancement factors due to turbulence for cross-size collisions. The enhancement factor η_E on the collision efficiency shows little dependence on R_λ and it is larger for both limiting cases $a_2/a_1 \rightarrow 1$ and $a_2/a_1 \rightarrow 0$. An enhancement up to a factor of 4 is observed for a_2/a_1 = 0.9 and a_1=20 μm with ϵ = 400 cm^2/s^3. For the limit of $a_2/a_1 \rightarrow 1$, the turbulent flow produces a fluctuating far-field condition. This combined with finite droplet inertia limits the effectiveness of hydrodynamic interactions in altering the droplet trajectories. This results in more collisions in turbulent air. For the other limit $a_2/a_1 \rightarrow 0$, the collision efficiency for the stagnant fluid case is very small. Minor modifications by turbulence such as local fluid shear and acceleration can affect the otherwise well-defined relative motion characterizing the small collision efficiency.

In general, the enhancement factor is smaller for larger a_1 as (1) the gravity plays a more dominant role in defining the disturbance flows and (2) the time scale for HI ($\propto R/(v_{p_1} - v_{p_2})$) is reduced. Air turbulence is

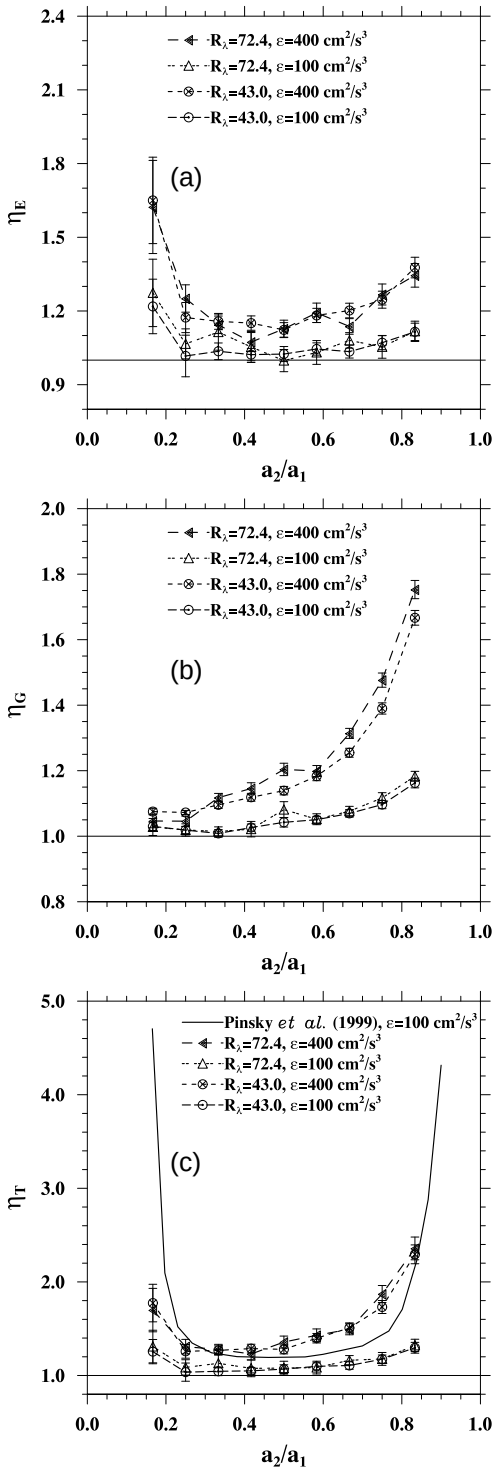

Figure 4: Turbulent enhancement factors for a_1=30 μm. (a) Enhancement factor η_E on the collision effi ciency, (b) enhancement factor η_G on the geometric collision kernel, and (c) total enhancement factor η_T ($\eta_E \eta_G$).

only effective in altering HI when i) the level of turbulence fluctuations at pair separation close to contact, as governed by ϵ, is comparable to $(v_{p_1} - v_{p_2})$, and ii) the hydrodynamic interaction time becomes comparable to τ_{p_2}, the inertial response time of the smaller droplet. The first condition may be roughly stated as

$$\frac{R(v_k/\eta)}{v_{p_1} - v_{p_2}} = \frac{9}{2}\frac{\rho}{\rho_w}\frac{\sqrt{\epsilon\nu}}{(a_1 - a_2)|\mathbf{g}|} \leq C_1, \qquad (12)$$

therefore, this condition implies a larger ϵ and a value of a_2/a_1 close to one. The second condition may be stated as

$$\frac{R}{(v_{p_1} - v_{p_2})\tau_{p_2}} = \left(\frac{9}{2}\frac{\rho}{\rho_w}\right)^2 \frac{\nu^2/|\mathbf{g}|}{{a_2}^2(a_1 - a_2)} \leq C_2. \qquad (13)$$

This condition favors the two limiting cases of $a_2/a_1 \rightarrow 0$ and $a_2/a_1 \rightarrow 1$. The above simple scaling arguments explain qualitatively the observed η_E behavior shown in fig. 4a. They also explain why the effect of turbulence on η_E decreases with increasing a_1 for a fixed a_2/a_1, as shown in Ayala (2005).

The enhancement factor η_G on the geometric collision kernel depends on R_λ and ϵ. In this case, the first condition, equation (12), should be satisfied for a large η_G, namely, large ϵ and $a_2/a_1 \rightarrow 1$. This qualitatively explains the general behavior in fig. 4b. Other conditions for enhanced geometric collision through particle clustering would be $\tau_p \sim \tau_k$ (Wang and Maxey 1993) and $F_p \equiv \tau_p {v_p}^2/\Gamma_{vort} = {\tau_p}^3|\mathbf{g}|^2/\nu \sim 1$ (Davila and Hunt 2001). For ν=0.17 cm^2/s, $|\mathbf{g}|$=980 cm/s^2, $\rho_w/\rho \approx$1000, the condition $F_p \sim 1$ implies

$$a_p \sim 21\mu\text{m}. \qquad (14)$$

The condition of $\tau_p \sim \tau_k$ yields

$$a_p(\mu m) \sim \frac{177}{[\epsilon(\text{in cm}^2/\text{s}^3)]^{0.25}}. \qquad (15)$$

For the range of dissipation rate in clouds ($\epsilon \leq 5000$ cm^3/s^2), we then expect that the preferential concentration is important for

$$21\mu\text{m} \geq a_p(\mu m) \leq \frac{177}{[\epsilon(\text{in cm}^2/\text{s}^3)]^{0.25}}.$$

This range is 21μm $\geq a_p(\mu m) \leq$ 56 μm for ϵ=100 cm^3/s^2 and 21μm $\geq a_p(\mu m) \leq$ 40 μm for ϵ=400 cm^3/s^2.

The overall enhancement factor by turbulence η_T is equal to $\eta_E\eta_G$ and typical results are shown in figure 4c. This can be in the range of 2 to 7 when $a_2/a_1 \sim 1$, for the two dissipation rates studied. The maximum overall enhancement of about 7 occurs for a_1=20 μm, a_2=18 μm, and ϵ=400 cm^3/s^2.

4. SUMMARY AND FUTURE WORK

A hybrid direct numerical simulation method was proposed for turbulent collisions of hydrodynamically-interacting particles. The method consists of direct simulation of an undisturbed turbulent flow, generated and maintained at large scales, and a analytical representation of local small-scale disturbance flows induced by the presence of particles. The no-slip boundary condition on each particle was satisfied when averaged over the surface of the particle (Wang et al. 2005a). The approach assumes that (1) the disturbance flow is very localized in space due to the dominant viscous effect; (2) there is a sufficient separation of length scales, namely, the particle size is much less than the smallest length scale (i.e., Kolmogorov length) of the undisturbed flow. The hybrid DNS approach, although very preliminary in nature, represents the most advanced approach available for treating turbulent collision of hydrodynamically-interacting particles (Wang *et al.* 2005b). It was found that air turbulence can moderately enhance both the geometric collision rate and collision efficiency. This moderate increase in the collection kernel can have a significant impact on the growth of cloud droplets (Xue *et al.* 2006). The approach has also been used to understand, in a turbulent flow, the enhanced settling of particles due to hydrodynamic interactions (Wang *et al.* 2006), a phenomenon observed experimentally by Aliseda *et al.* (Aliseda *et al.* 2003).

Several implementation issues of the hybrid approach were discussed in Ayala *et al.* (2006) to ensure numerical accuracy and consistency of the approach, including the determination of time step size, the hydrodynamic interaction radius, and iterative method for the disturbance velocities. Guidelines have been developed for the time step size and the hydrodynamic interaction radius.

As was pointed out in the Introduction, the method shown here represents a first step towards a rigorous modeling of a three-way coupling system. Here we comment on future directions to further develop the hybrid DNS approach. First, the hydrodynamic interaction radius needs to be formulated in terms of a more realistic representation of the far-field disturbance flow with a consideration of fluid inertial effects in both the disturbance flow and the background turbulence. This would eliminate the need to adjust H in our approach. Second, the improved superposition method does not correctly model the lubrication force between two particles, as pointed out in Wang et al. (2005a). Analytical methods using multipole techniques at large separations and lubrication expansion for small separations (Jeffrey and Onishi 1984; Davis 1984; Chun and Koch 2005) are the logical next step to improve our approach. Finally, when the minimum separation between two particles approaches the mean free path of fluid medium, non-continuum effects (Hocking 1973; Sundararajakumar and Koch 1996) will have to be included.

Acknowledgments This study has been supported by the National Science Foundation through

grants ATM-0114100 and ATM-0527140, and by the National Center for Atmospheric Research (NCAR).

References

Aliseda, A., A. Cartellier, F. Hainaux, J.C. Lasheras, Effect of preferential concentration on the settling velocity of heavy particles in homogeneous isotropic turbulence, J. Fluid Mech. 468 (2002) 77-105.

Allen, M.P., D.J. Tildesley, Computer Simulation of Liquids, Oxford University Press, 1989.

Ayala, O., 2005: Effects of turbulence on the collision rate of cloud droplets. Ph.D. dissertation, University of Delaware, Newark, Delaware, U.S.A.

Ayala, O., W. W. Grabowski, and L.P. Wang, A hybrid approach for simulating turbulent collisions of hydrodynamically-interacting particles, J. Comput. Phys., in review.

Batchelor, G.K., Sedimentation in a dilute dispersion of shperes. J. Fluid Mech. 52 (1972) 245-268.

Batchelor, G.K., Sedimentation in a dilute polydisperse system of interacting spheres. Part 1. General theory. J. Fluid Mech. 119 (1982) 379-408.

Beard, K.V., S.N. Grover, Numerical collision efficiencies for small raindrops colliding with micron size particles, J. Atmos. Sci. 31 (1974) 543-550.

Brady, J.F., G. Bossis, Stokesian Dynamics, Annu Rev. Fluid Mech. 20 (1988) 111-157.

Brenner, M.P., Screening mechanisms in sedimentation, Phys. Fluids 11 (1999) 754-772.

Chun, J. and D.L. Koch, Coagulation of monodisperse aerosol particles by isotropic turbulence, Phys. Fluids 17 (2005) 027102.

Collins, L.R. and A. Keswani, 2004, Reynolds number scaling of particle clustering in turbulent aerosols. *New J. of Phys.*, **6**, Art. No. 119.

Crowe, C., M. Sommerfeld, Y. Tsuji, Multiphase flows with droplets and particles, CRC press, New York, 1998.

Davila, J., and J.C.R. Hunt, 2001: Settling of small particles near vortices and in turbulence. *J. Fluid Mech.*, **440**, 117-145.

Davis, M.H., J.D. Sartor, Theoretical collision efficiencies for small cloud droplets in Stokes flow. Nature 215 (1967) 1371-1372.

Davis, R.H., The rate of coagulation of a dilute polydisperse system of sedimenting spheres, J. Fluid Mech. 145 (1984) 179-199.

Davis, R.H., Hydrodynamic diffusion of suspended particles: a symposium, J. Fluid Mech. 310 (1996) 325-335.

Elghobashi, S., On predicting particle-laden turbulent flows. Appl. Sci. Res. 52 (1994) 309-329.

Eswaran, E., S.B. Pope, An examination of forcing in direct numerical simulations of turbulence, Comp. Fluids 16 (1988) 257-278.

Hinch, E.J., Sedimentation of small particles. In *Disorder and Mixing* (Ed. E. Guyon, J-P Nadal and Y. Pomeau), Kluwer Academic Publishers, 153-161, 1988.

Hocking, L.M., Effect of slip on motion of a sphere close to a wall and of 2 adjacent spheres, J. Eng. Math. 7 (1973) 207-221.

Hu, K., R. Mei, Effect of inertia on the particle Collision Coefficient in Gaussian Turbulence. CDROM Proceedings, ASME Fluid Engineering Div. Summer Meeting, 1997.

Ichiki, K., Improvement of the Stokesian Dynamics method for systems with a finite number of particles, J. Fluid Mech. 452 (2002) 231-262.

Ichiki, K., J.F. Brady, Many-body effects and matrix inversion in low Reynolds number hydrodynamics, Phys. Fluids 13 (2001) 350-353.

Jeffrey, D.J., Y. Onishi, Calculation of the resistance and mobility functions for two unequal rigid spheres in low-Reynolds-number flow, J. Fluid Mech. 139 (1984) 261-290.

Kim, S. and S. J. Karrila, Microhydrodynamics, Principles and Selected Applications, Butterworth-Heinemann, Boston, 507pp, 1991.

Klett, J., M. Davis, Theoretical collision efficiencies of cloud droplets at small Reynolds numbers, J. Atmos. Sci. 30 (1973) 107-117.

Koch, D.L., E.S.G. Shaqfeh, Screening in sedimenting suspensions. J. Fluid Mech. 224 (1991) 275-303.

Ladd, A.J.C., Hydrodynamic screening in sedimenting suspensions of non-Brownian spheres. Phys. Rev. Lett. 76 (1996) 1392-1395.

Langmuir, I., The production of rain by a chain reaction in cumulus clouds at temperature above frezzing, J. Meteorology 5 (1948) 175-192.

Lin, C., S. Lee, Collision efficiency of water drops in the atmosphere, J. Atmos. Sci. 32 (1975) 1412–1418.

Lin, C.L., S.C. Lee, The effect of vertical separation on droplet collision efficiency (Reply to comments by Cataneo and Semonin). J. Atmos. Sci. 33 (1976) 1826-1827.

Moin, P., K. Mahesh, Direct numerical simulation: A tool in turbulence research, Annu. Rev. Fluid Mech. 30 (1998) 539-578.

Nicolai, H., B. Herzhaft, E.J. Hinch, L. Oger, E. Guazelli, Particle velocity fluctuations and hydrodynamic self-diffusion of sedimenting non-Brownian spheres, Phys. Fluids 7 (1995) 12-23.

Noh, Y., H.J.S. Fernando, The transition in the sedimentation pattern of a particle cloud. Phys. Fluids. 5 (1993) 3049-3055.

Pinsky, M.B., A. P. Khain, Turbulence effects on droplet growth and size distribution in clouds - A review. J. Aerosol Sci. 28 (1997) 1177-1214.

Pinsky, M., A. Khain, and M. Shapiro, Collisions of small drops in a turbulent flow. Part I. Collision efficiency. Problem formulation and preliminary results, J. Atmos. Sci. 56(15) (1999) 2585-2600.

Pruppacher, H.R., J.D. Klett, Microphysics of Clouds and Precipitation, Klumer Academic Publishers, AH Dordrecht, The Netherlands, 1997.

Ramaswamy, S., Issues in the statistical mechanics of steady sedimentation. Adv. in Physics 50 (2001) 297-341.

Sangani, A.S., G.B. Mo, An O(N) algorithm for Stokes and Laplace interactions of particles, Phys. Fluid 8 (1996) 1990-2010.

Shafrir, U., M. Neiburger, Collision efficiencies of two spheres falling in a viscous medium, J. Geophys. Res. 68 (1963) 4141-4147.

Shaw, R.A., Particle-turbulence interactions in atmospheric clouds. Annu. Rev. Fluid Mech. 35 (2003) 183-227.

Sierou, A., J.F. Brady, Accelerated Stokesian Dynamics simulations, J. Fluid Mech. 448 (2001) 115-146.

Sundaram, S., L.R. Collins, Collision Statistic in an Isotropic, Particle-Laden Turbulent Suspension. J. Fluid Mech. 75 (1997) 337-350.

Sundararajakumar, R.R., D.L. Koch, Non-continuum lubrication flows between particles colliding in a gas, J. Fluid Mech. 313 (1996) 283-308.

Vaillancourt, P.A., and M. K. Yau, Review of particle-turbulence interactions and consequences for cloud physics. Bull. Amer. Meteor. Soc. 81 (2000) 285-298.

Wang, L.P., M.R. Maxey, Settling velocity and concentration distribution of heavy particles in homogeneous isotropic turbulence, J. Fluid Mech., 256 (1993) 27-68.

Wang, L.P., A. Wexler, Y. Zhou, Statistical mechanical description and modelling of turbulent collision of inertial particles. J. Fluid Mech. 415 (2000) 117-153.

Wang, L.P., O. Ayala, W.W. Grabowski, On improved formulations of the superposition method, J. Atmos. Sci. 62 (2005a) 1255-1266.

Wang, L.P., O. Ayala, S.E. Kasprzak, W.W. Grabowski, Theoretical formulation of collision rate and collision efficiency of hydrodynamically-interacting cloud droplets in turbulent atmosphere, J. Atmos. Sci. 62 (2005b) 2433-2450.

Wang, L.P., O. Ayala, W. W. Grabowski, Effects of aerodynamic interactions on the motion of heavy particles in a bidisperse suspension, J. Fluid Mech. (to appear), 2006.

Xue, Y, W. W. Grabowski, L.P. Wang, 2006, Growth of cloud droplets by turbulent collision-coalescence. 12th Conference on Cloud Physics, 10-14 July 2006, Madison, WI.

Yang, T.S. and S.S. Shy, 2005 Two-way interaction between solid particles and homogeneous air turbulence: particle settling rate and turbulence modification measurements. *J. Fluid Mech.* **526**, 171-216.